

Received September 23, 2019, accepted October 4, 2019, date of publication October 14, 2019, date of current version October 28, 2019.

Digital Object Identifier 10.1109/ACCESS.2019.2947287

Low-Cost Precise Vehicle Localization Using Lane Endpoints and Road Signs for Highway Situations

MI JIN CHOI¹, JAE KYU SUHR¹, (Member, IEEE), KYOUNGTAEK CHOI¹,
AND HO GI JUNG², (Senior Member, IEEE)

¹School of Intelligent Mechatronics Engineering, Sejong University, Seoul 05006, South Korea

²Department of Electronic Engineering, Korea National University of Transportation, Chungju-si 27469, South Korea

Corresponding author: Ho Gi Jung (hogijung@ut.ac.kr)

This research was supported by a Grant (code 19TLRP-B101406-05) from Development of Cooperative Automated Driving Highway Systems Program funded by Ministry of Land, Infrastructure and Transport of Korean Government.

ABSTRACT In highways, lane markings are undoubtedly the most widely used landmarks for vehicle localization. However, they have a drawback in that they lack information on longitudinal position estimation and ego-lane identification. To alleviate this drawback, this paper presents a practical vehicle localization system for highways. The proposed system utilizes lane endpoints to enhance longitudinal position accuracy and road signs to improve the ego-lane identification accuracy. This system efficiently fuses the lane markings, lane endpoints and road signs along with a digital map and other low-cost sensors in a particle filter framework. Since it only uses low-cost sensors such as a monocular front-view camera, in-vehicle wheel speed and yaw rate sensors, as well as a low-end global positioning system (GPS), it is ready to mount on mass-produced vehicles. In the experiment, the proposed system was quantitatively evaluated using a dataset obtained while driving on 40 km stretch of highway, and outperformed previous approaches by showing a lateral position error of less than 0.12 m and a longitudinal position error of less than 0.25 m in terms of root mean square error (RMSE).

INDEX TERMS Highway autonomous driving, lane endpoint, particle filter, road sign, sensor fusion, vehicle localization.

I. INTRODUCTION

In recent years, the technologies of advanced driver assistance systems (ADAS) and autonomous driving have developed rapidly. Vehicle localization is one of the key components of these technologies with other components such as perception, planning, and control. Therefore, precise vehicle localization is attracting attention as an essential requirement for autonomous vehicles [1]–[3]. Global navigation satellite systems (GNSS) are the most widely used technique for vehicle localization. However, it can generate large localization errors when signals are reflected or blocked in urban canyons or tunnels. Many studies have been conducted to alleviate this problem [4]–[6], and the fusion of GNSS and dead reckoning (DR) has become a representative approach. However, its performance can be degraded when its errors accumulate

when the GNSS signal is reflected or blocked for a long period of time.

To overcome the drawbacks of the GNSS-DR, localization methods utilizing a perception sensor with a digital map have been extensively researched [7]–[11]. These methods estimate the position of the ego-vehicle by matching the landmarks found by the perception sensor and the corresponding landmarks stored in the digital map. A variety of landmarks have been used for vehicle localization, and road surface markings are one of the most widely used landmarks. From the viewpoint of the perception sensor, road surface markings are easy to detect since their shapes are simple and standardized and their color and reflectivity are distinctive from those of the road surface. Among road surface markings, lane markings are undoubtedly the most widely used landmarks [4], [6], [11]–[13]. Although lane markings provide accurate in-lane lateral positions, it lacks information on longitudinal position and ego-lane identification. To alleviate

The associate editor coordinating the review of this manuscript and approving it for publication was Razi Iqbal .

these drawbacks, methods utilizing other road surface markings such as stop lines, crosswalks, arrows, and letters have been suggested. Since those road surface markings frequently appear on urban roads, they are useful in urban situations. However, in highway situations, stop lines and crosswalks rarely exist, and arrows and letters only appear in specific areas such as intersections [12], and their usability is quite limited in highway situations.

Therefore, this paper proposes a practical vehicle localization system that alleviates the drawbacks of lane markings in highway situations. To enhance the longitudinal position accuracy, the proposed system utilizes lane endpoints. Our previous paper introduces a method to efficiently detect lane endpoints but does not present a method to use them for vehicle localization purposes [12]. Although lane markings and lane endpoints can improve in-lane position accuracy, it cannot enhance the ego-lane identification accuracy because the lane endpoints appear in multiple lanes. In highway situations, the ego-lane identification task becomes more difficult compared with urban situations due to a large number of lanes, repetitive road structures, and a simple background. Two main approaches have been used to identify ego-lanes. One approach recognizes road boundaries to identify ego-lanes [14]–[16]. But this approach becomes infeasible if the road is too wide to capture in the camera's field-of-view or the road is too crowded for the camera to observe the road boundaries. The other approach detects types of arrows in ego and adjacent lanes and identifies ego-lanes based on their types [4], [10]. But in highway situations, since arrows seldom appear, and multiple lanes have the same type of arrows, this approach becomes impractical. To improve ego-lane identification accuracy, the proposed system utilizes road signs. The road signs are useful for ego-lane identification because their positions are different in images when they are captured in different lanes.

Other vehicles rarely occlude them because they are installed in high positions. The proposed system efficiently fuses lane markings, lane endpoints, and road signs along with a digital map and other low-cost sensors in the particle filter framework. Here, lane endpoints are used to enhance the longitudinal position accuracy and road signs are used to improve the ego-lane identification accuracy. Also, the landmarks used in the proposed system are detected by our previously developed methods: the lane and lane endpoint detection method [12], and the road sign detection method [17]. This system is ready to mount on mass-produced vehicles since it only uses low-cost sensors such as a monocular front-view camera, in-vehicle wheel speed and yaw rate sensors, and a low-end global positioning system (GPS). In the experiment, the proposed system was quantitatively evaluated using a dataset obtained while driving on 40 km of highway, and outperformed previous methods by showing a localization accuracy of less than 0.3 m in root-mean square-error (RMSE) and execution time of 4.34 ms.

The proposed system has the following contributions:

- 1) It suggests a method that efficiently combines lane markings, lane endpoints, and road signs as landmarks for vehicle localization purposes in highway situations.
- 2) It achieves accurate vehicle localization results (less than 0.3 m) and ego-lane identification results (almost 100%) while requiring a small amount of computational cost (4.34 ms).
- 3) It is ready to be applied to mass-produced vehicles since it utilizes only low-cost sensors that have been already mounted on off-the-shelf vehicles.

The rest of this paper is organized as follows: Section 2 presents related research. Section 3 introduces an overview of the proposed system. Sections 4 and 5 explain the landmark detection method used for the proposed system and the particle filtering-based vehicle localization, respectively. Section 6 describes the experimental results and analyses. Finally, this paper is concluded in Section 7.

II. RELATED WORK

According to information obtained by the perception sensor and contained in the digital map, localization methods utilizing a perception sensor with a digital map can be categorized into a feature point-based approach [5], [7]–[9] and a road facility-based approach [4], [6], [10], [11], [17]–[24], [41]. The feature point-based approach finds feature points using cameras and matches them with the corresponding feature points contained in the digital map. When feature points are reliably found and matched, it can achieve high localization accuracy. However, its performance can be degraded by appearance changes of surrounding obstacles and it needs a large amount of storage for the digital map to contain numerous feature points and their descriptors. The road facility-based approach extracts road facilities such as road surface markings [19]–[24], [41], traffic lights [18], traffic signs [25], road signs [17], [40], and streetlights [26] and matches them with the corresponding road facilities contained in the digital map. This approach requires a small amount of storage for the digital map compared with the feature point-based approach because the digital map contains simplified shapes, types, and locations of the road facilities. Since the road facilities are designed to be visually distinctive and under government control, they are relatively easy to be recognized by perception sensors and their locations and appearance are seldom changed without permission. For these reasons, the road facility-based approach can be considered more suitable for vehicle localization in highway situations. Since the proposed system is categorized into the road facility-based approach, this section focuses on previous methods in this approach.

A variety of landmarks have been used for the road facility-based approach, and road surface markings are one of the most widely used landmarks for vehicle localization [4], [11], [19]–[24], [41]. From the viewpoint of the perception sensor, road surface markings are relatively easy to detect since their shapes are simple and standardized, and their color and reflectivity are distinctive from those of the

road surface. But usability of these landmarks can decrease when they are worn or covered with snow. The methods using road surface markings can be categorized into signal-level, feature-level, and symbol-level approaches based on the level of information being used.

The signal-level approach [19], [20] utilizes raw data of the road surface markings acquired by the perception sensor. The feature-level approach [21]–[23] extracts features of the road surface markings from raw data of the perception sensor. The signal-level and feature-level approaches do not require much effort to process the outputs of the perception sensors. But they require a high computational cost for the matching procedure and a large amount of storage for the digital map because the raw data and features extracted from it includes a lot of information. The symbol-level approach [4], [10], [24], [41] detects various road surface markings and matches them with those contained in the digital map. This approach requires a low computational cost for the matching procedure and a small amount of storage for the digital map because it simply matches and stores types and positions of the symbols. However, it does require extra computational costs to detect target symbols.

The most popular symbol used in the symbol-level approach is lane markings. Nedeveschi *et al.* [10], Lu *et al.* [24], Gu *et al.* [41], and Suhr *et al.* [4] used lane markings for vehicle localization purposes. In a similar manner, curbs and guardrails have been used instead of lane markings [27], [28]. However, lane markings have a drawback in that they lack information on both longitudinal position estimation and ego-lane identification. To alleviate this drawback, crosswalks [29], stop lines [10], arrows [4], and letters [30] have been utilized. These are useful in urban situations because they are frequently observed on urban roads. But in highway situations, crosswalks and stop lines seldom exist, and arrows and letters rarely appear. In our previous work [12], the distributions of road surface markings on approximately 40 km of Korean highway situations were analyzed. It was found that there are no crosswalks and stop lines on highways, and arrows and letters are observed only in approximately 3% of the entire route. Furthermore, the longest section that does not include any arrows and letters was up to 7.8 km in length. This analysis shows that crosswalks, stop lines, arrows, and letters have limitations for alleviating the drawback of lane markings in highway situations.

Road facilities other than road surface markings have also been utilized for vehicle localization purposes. Traffic signs and streetlights have been used as landmarks for enhancing localization accuracy. Those landmarks are less occluded because they are located higher than the surrounding vehicles. Unlike road surface markings, they are not easily worn and are seldom covered with snow. However, it is difficult to obtain accurate vehicle localization results when using traffic signs or streetlights alone because they do not frequently appear on the road like lane markings. Although streetlights appear on the road more often than traffic signs, high-end

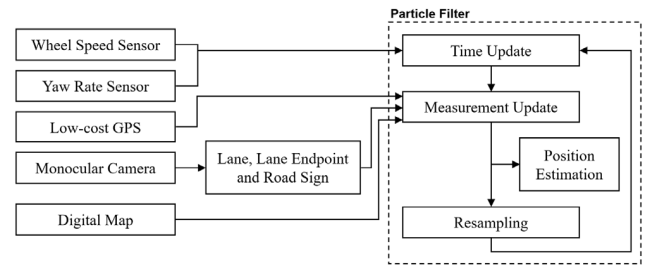


FIGURE 1. Overview of the proposed system.

perception sensors such as lidars are required to reliably detect them [26]. Li *et al.* [25] calculated the 3D position of a traffic sign detected by a monocular camera using a digital map and proposed a particle filter-based localization method using lane markings and traffic signs. Kim and Park [16] suggested a method that detects traffic signs using a stereo camera and identified ego-lanes based on lateral offsets from the detected traffic signs. Kim *et al.* [26] presented a method that uses streetlights detected by a lidar as well as lane markings.

To develop a practical vehicle localization system, this paper proposes a system that only uses landmarks that can be detected by a low-cost monocular front-view camera, which has already been mounted on numerous off-the-shelf vehicles. To improve the localization accuracy, the proposed system utilizes a combination of lane endpoints and road signs that has not been utilized for vehicle localization purposes. Although the proposed system uses only low-cost sensors and requires a small amount of computational cost, it achieves accurate vehicle localization results in highway situations.

III. SYSTEM OVERVIEW

Fig. 1 shows a block diagram of the proposed system. The left part of this diagram shows low-cost sensors and a digital map used for the proposed system. Its right part shows the particle filter-based vehicle localization that consists of four steps: time update, measurement update, position estimation, and resampling. The time update step predicts the distribution of the vehicle state using the wheel speed and yaw rate sensors. The measurement update step corrects the distribution of the vehicle state using a low-cost GPS, landmarks (lanes, lane endpoints, and road signs) detected by the monocular front-view camera, and a digital map. The position estimation step determines the vehicle position based on the distribution of the vehicle states. The resampling step resamples particles to prevent the situation where the probability mass is concentrated on a few particles.

IV. LANDMARK DETECTION

A. LANE AND LANE ENDPOINT DETECTION

Lanes and lane endpoints are detected based on the method proposed in [12]. This method first extracts lane candidate pixels using a top-hat filter and detects left and right lanes based on random sample consensus (RANSAC)-based line

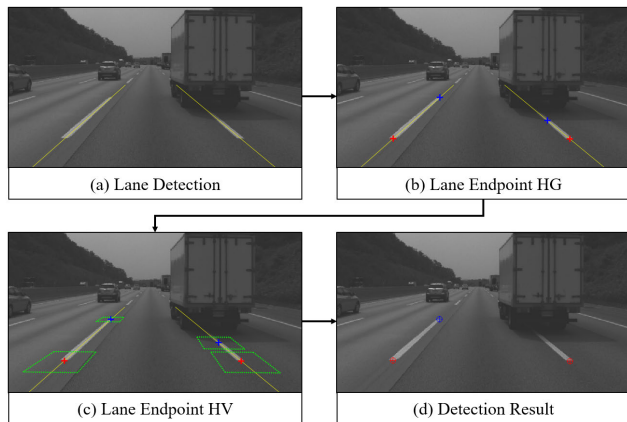


FIGURE 2. Lane endpoint detection procedure.

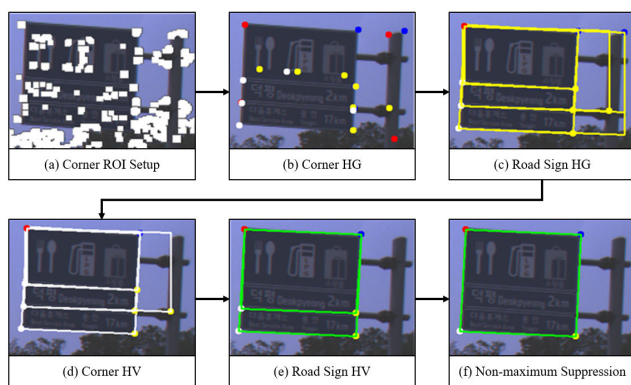


FIGURE 3. Road sign detection procedure.

estimation. Yellow lines in Fig. 2(a) show a lane detection result. More sophisticated methods can also be used for lane detection [42]. After detecting left and right lanes, profiles of the top-hat filter response are acquired along the left and right lanes. Lane endpoint candidates are found by extracting local minima and maxima from differentiation results of the profiles because they indicate the locations where bright values abruptly change. Red and blue crosses in Fig. 2(b) shows an example of the lane endpoint candidates generated by the lane endpoint hypothesis generation (HG). Neighboring areas around the lane endpoint candidates are converted into bird's-eye view images and verified by a simple but efficient classifier that uses a histogram of oriented gradients (HOG) and the support vector machine (SVM). Green rectangles in Fig. 2(c) show the neighboring area of lane endpoint candidates used for the lane endpoint hypothesis verification (HV). Red and blue circles in Fig. 2(d) show the final lane endpoint detection result after the verification. Finally, the positions of the detected lane endpoints are estimated by using intrinsic and extrinsic parameters of the front-view camera.

B. ROAD SIGN DETECTION

Road signs are detected based on the method proposed in [17]. The road sign detection procedure consists of six steps as shown in Fig. 3. In order to reduce the computational cost,

this method first selects regions of interest (ROIs). Corners are extracted by the method called features from accelerated segment test (FAST) and the regions around the extracted corners are set to ROIs. White squares in Fig. 3(a) are the selected ROIs. The corner HG step is conducted based on the selected ROIs. In this step, a Viola-Jones detector with local binary pattern (LBP) features finds four types of corners within the selected corner ROIs [31], [32]. The Viola-Jones detector is trained to find four types of corners: in Fig. 3(b), top-left, top-right, bottom-left, and bottom-right corners depicted with red, blue, white, and yellow dots, respectively. Once four types of corners are found, the road sign HG step combines several corners that satisfy predetermined geometric constraints and produces road sign hypotheses. Yellow rectangles shown in Fig. 3(c) indicate the generated road sign hypotheses. After the road sign HG step, the corner HV step examines the corners composing the road sign hypotheses by using the SVM classifier with HOG features [33], [34]. The dots and rectangles shown in Fig. 3(d) show the corner and road sign hypotheses remained after corner verification. The road sign HV step examines the road sign hypotheses remained after corner verification by using the SVM classifier with HOG features. Two rectangles in Fig. 3(e) indicate the road sign hypotheses remained after the road sign verification. Finally, the non-maximum suppression (NMS) step determines the most reliable road sign when multiple road signs overlap. Fig. 3(f) shows an example result of the road sign detection.

V. PARTICLE FILTERING-BASED VEHICLE LOCALIZATION

The proposed system utilizes the particle filter to localize the ego-vehicle by fusing in-vehicle motion sensors, low-cost GPS, monocular front-view camera, and a digital map. The particle filter has been widely used for vehicle localization purposes because it can fuse various sensors in a simple way and be applied to nonlinear or non-Gaussian system [4], [6]. As aforementioned in Fig. 1, the particle filter consists of four steps: time update, measurement update, position estimation, and resampling. The system repeats these four steps. This chapter explains all those four steps in detail.

The particle filter estimates the probability distribution of the current state variables from the measured information. The probability distribution is represented by a set of M particles. In this paper, the n -th particle at time t is denoted by \mathbf{x}_t^n ($1 \leq n \leq M$) and consists of three values as

$$\mathbf{x}_t^n = [x_t^n \quad y_t^n \quad \theta_t^n]^T \quad (1)$$

where x_t^n and y_t^n indicate the 2D location and θ_t^n indicates the heading angle. Initial particles are generated based on the probability density function of the initial state, which is derived by the ego-vehicle location and heading angle provided by the low-cost GPS.

A. TIME UPDATE

The time update step predicts the distribution of the vehicle state based on the velocity motion model [35]. This motion model utilizes two velocities: a translational velocity

(vehicle speed, v) and a rotational velocity (yaw rate, ω) acquired by the wheel speed and yaw rate sensors, respectively. Predicted particle $\hat{\mathbf{x}}_{t|t-1}^n$ is generated as

$$\begin{aligned} \hat{\mathbf{x}}_{t|t-1}^n &= \begin{bmatrix} \hat{x}_{t|t-1}^n \\ \hat{y}_{t|t-1}^n \\ \hat{\theta}_{t|t-1}^n \end{bmatrix} \\ &= \begin{bmatrix} \hat{x}_{t-1|t-1}^n - \tilde{v}/\tilde{\omega} \sin(\hat{\theta}_{t-1|t-1}^n) + \tilde{v}/\tilde{\omega} \sin(\hat{\theta}_{t-1|t-1}^n + \tilde{\omega}\Delta t) \\ \hat{y}_{t-1|t-1}^n + \tilde{v}/\tilde{\omega} \cos(\hat{\theta}_{t-1|t-1}^n) - \tilde{v}/\tilde{\omega} \cos(\hat{\theta}_{t-1|t-1}^n + \tilde{\omega}\Delta t) \\ \hat{\theta}_{t-1|t-1}^n + \tilde{\omega}\Delta t \end{bmatrix} \\ \tilde{v} &= v + \mathbf{sample}(\sigma_v^2), \quad \tilde{\omega} = \omega + \mathbf{sample}(\sigma_\omega^2) \end{aligned} \quad (2)$$

where the overhead tilde (\sim) represents a variable perturbed by an additional random noise and $\mathbf{sample}(\sigma^2)$ is a function that generates a random sample from a zero-mean Gaussian distribution with variance σ^2 . σ_v^2 and σ_ω^2 are variances for wheel speed and yaw rate noises, respectively. Since the particle filter uses a finite number of particles, it has a limitation of representing a high-dimensional probability distribution. Due to this limitation, the particle filter can suffer from the particle degeneracy problem [36], [37]. To avoid this problem, this paper uses a jittering technique [36].

B. MEASUREMENT UPDATE

The measurement update step corrects the distribution of the vehicle state using a low-cost GPS, landmarks detected by the camera, and a digital map. As landmarks, this paper uses lanes, lane endpoints, and road signs. The goal of the measurement update can be thought of as calculating the weight for each particle. The final weight (w_t^n) of the predicted particle ($\hat{\mathbf{x}}_{t|t-1}^n$) is calculated as

$$w_t^n = w_{t-1}^n \cdot w_{G,t}^n \cdot w_{L,t}^n \cdot w_{E,t}^n \cdot w_{S,t}^n \quad (3)$$

where $w_{G,t}^n$, $w_{L,t}^n$, $w_{E,t}^n$, and $w_{S,t}^n$ are the weights obtained from the low-cost GPS, lane, lane endpoint, and road sign, respectively. If some landmarks are unobservable, corresponding weights are set to 1.0. It means that the particles are updated only using the observed landmarks. If no landmark is observable, the proposed system estimates the vehicle position based on GPS and in-vehicle motion sensors.

The weight for the low-cost GPS, $w_{G,t}^n$ is calculated based on the difference between the 2D location measured by the low-cost GPS and that of the predicted particle. This weight is modeled by a multivariate Gaussian distribution as

$$w_{G,t}^n = \frac{1}{2\pi\sqrt{\det(\Sigma_G)}} \exp \left\{ -\frac{1}{2} (\hat{\mathbf{p}}_t^n - \mathbf{p}_{G,t})^T \Sigma_G^{-1} (\hat{\mathbf{p}}_t^n - \mathbf{p}_{G,t}) \right\} \quad (4)$$

where $\mathbf{p}_{G,t} (= [x_{GPS,t} \ y_{GPS,t}]^T)$ is a 2D location measured by the low-cost GPS and $\hat{\mathbf{p}}_t^n (= [\hat{x}_{t|t-1}^n \ \hat{y}_{t|t-1}^n]^T)$ is a 2D location of the predicted particle. Σ_G is set to a 2×2 diagonal matrix. Fig. 4(a) shows an example of the probability density

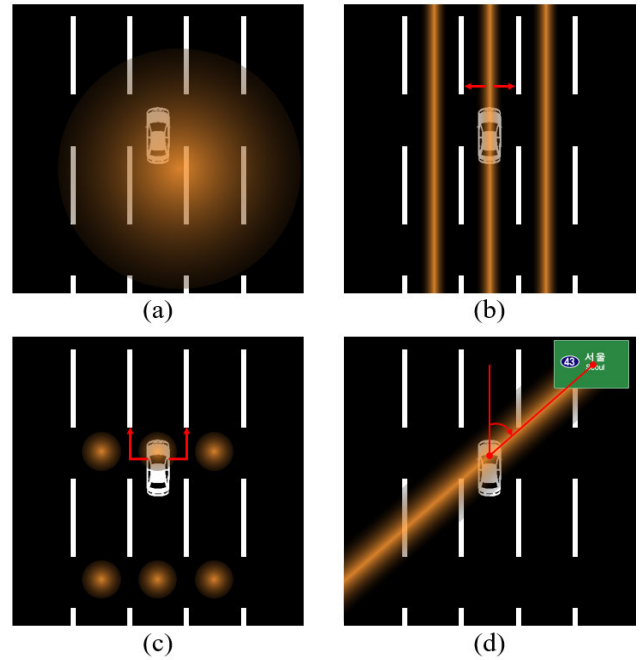


FIGURE 4. Probability distribution functions for the (a) low-cost GPS-based measurement update, (b) lane-based measurement update, (c) lane endpoint-based measurement update, and (d) road sign-based measurement update. The heading angles of the predicted particles are assumed to be parallel with the lane direction when drawing these figures for convenience.

distribution of the low-cost GPS-based measurement update in orange. Vivid orange-colored locations have large values. In this figure, a three-lane road with dashed lane markings is depicted, and the center of the distribution indicates the 2D location measured by the low-cost GPS.

The weights for the landmarks are calculated by matching the landmarks detected by the camera and those stored in the digital map. In the case of a lane, the lateral offset of the ego-vehicle with respect to the driving lane is used. The weight for the lane, $w_{L,t}^n$ is calculated based on the difference between the lateral offset measured by the camera, $l_{D,t}$ and the lateral offset of the predicted particle in the digital map, \hat{l}_t^n as

$$w_{L,t}^n = \frac{1}{\sqrt{2\pi\sigma_L^2}} \exp \left\{ -\frac{(\hat{l}_t^n - l_{D,t})^2}{2\sigma_L^2} \right\} \quad (5)$$

The lateral offset of the predicted particle, \hat{l}_t^n is calculated by using the predicted particle and the lane that includes the predicted particle in the digital map. σ_L^2 is the variance for the lateral offset of the lane. Fig. 4(b) shows an example of the probability density distribution of the lane-based measurement update in the case where $l_{D,t}$ is measured to be at the center of the driving lane. This distribution has larger values at the centers of all lanes.

In case of the lane endpoint, the lateral and longitudinal offsets of the lane endpoint with respect to the ego-vehicle are used. The weight for the lane endpoint, $w_{E,t}^n$ is calculated

based on the difference between the 2D offset measured by the camera, $\mathbf{e}_{D,t}$ and the 2D offset of the predicted particle in the digital map, $\hat{\mathbf{e}}_t^n$ as

$$w_{E,t}^n = \frac{1}{2\pi\sqrt{\det(\Sigma_E)}} \exp \left\{ -\frac{1}{2} (\hat{\mathbf{e}}_t^n - \mathbf{e}_{D,t})^T \Sigma_E^{-1} (\hat{\mathbf{e}}_t^n - \mathbf{e}_{D,t}) \right\} \quad (6)$$

The 2D offset of the predicted particle, $\hat{\mathbf{e}}_t^n$ is calculated using the predicted particle and the lane endpoint in the digital map, which corresponds to the lane endpoint detected by the camera. The nearest neighbor matching is used when pairing the lane endpoints detected by the camera and stored in the digital map. Only lane endpoints of the same type are matched. Σ_E is the covariance matrix for the 2D offset of the lane endpoint. Fig. 4(c) shows an example of the probability density distribution of the lane endpoint-based measurement update in cases where two lane endpoints are detected. This distribution has larger values at the locations that give the 2D offsets similar to the 2D offset measured by the camera.

In the case of the road sign, unlike the lane and lane endpoint, it is difficult to use the offset to the road sign. This is because the 3D position of the road sign cannot be reliably calculated when using the monocular front-view camera. Lanes and lane endpoints are located on the ground plane and they can be captured by the camera when their locations are close to the camera. However, the road signs are usually located at 5.0 m above the ground plane and their sizes are relatively large. Thus, the whole road sign can be captured by the camera with limited field-of-view only when its location is far from the camera. In the case of using a monocular camera, 3D position estimation error dramatically increases while the distance to the target object from the camera increases. We have tried to estimate the 3D positions of the road signs and used them for the measurement update, but this approach produces a relatively large vehicle localization error due to the aforementioned problem. Therefore, instead of using the 3D position of the road sign, we decided to use the directional information of the road sign that is the angle between the driving direction of the ego-vehicle and the incidence angle of the road sign's center point. This approach produces reliable results because the monocular camera has an advantage in angle estimation thanks to its high angular resolution. The weight for the road sign, $w_{S,t}^n$ is calculated based on the difference between the angle of the road sign measured by the camera, $\phi_{D,t}$ and the angle of the road sign calculated by the predicted particle in the digital map, $\hat{\phi}_t^n$ as

$$w_{S,t}^n = \frac{1}{\sqrt{2\pi\sigma_S^2}} \exp \left\{ -\frac{(\hat{\phi}_t^n - \phi_{D,t})^2}{2\sigma_S^2} \right\} \quad (7)$$

$\hat{\phi}_t^n$ is calculated using the predicted particle and the road sign in the digital map, that corresponds to the road sign detected by the camera. When multiple road signs are presented, a Hungarian algorithm is used for pairing them [38]. σ_S^2 is the variance for the angle of the road sign. Fig. 4(d) shows an

example of the probability density distribution of the road sign-based measurement update when the road sign appears on the right side of the ego-vehicle. This distribution has larger values at the center of the line that connects the center point of a road sign and the camera. If only a road sign is used for vehicle localization, it is impossible to determine the ego-lane. However, if the road sign is combined by lane endpoints that provide a precise longitudinal position, the ego-lane can clearly be identified.

In case where multiple road signs exist at similar locations, this system still properly works because it can detect multiple road signs and matches them with nearby road signs in the digital map. In detail, the road sign detector finds all road signs captured by a front-view camera. Once road signs are detected, reference road sign locations near the ego-vehicle location are retrieved from the digital map. After that, the detected road signs and retrieved road signs are matched by their locations. Finally, the matching results are used for calculating the road sign-based weight in (7).

C. POSITION ESTIMATION AND RESAMPLING

The position estimation step determines the position of the ego-vehicle based on the distribution of the vehicle states. In this paper, the ego-vehicle position is determined by the minimum mean square error (MMSE) estimator that can be approximated by the weighted mean of the particles [6]. The resampling step resamples particles to prevent a situation where the probability mass is concentrated on a few particles. This paper uses a low-variance sampling method for resampling [4].

VI. EXPERIMENTS

A. EXPERIMENTAL ENVIRONMENT

The proposed system was evaluated using a dataset that includes a total of 40 km of driving on Korean highways. In detail, this route is from the Seoul tollgate to the Hobeop junction of the Yeongdong and Gyeongbu highway in South Korea as shown in the first row of Fig. 5. Since the test route is quite long, it is divided into two subsets: DB 1 and DB 2. In the first row of Fig. 5, blue and red points indicate the routes for DB 1 and DB 2, respectively. Detailed explanations on DB 1 and DB 2 are presented in Table 1. The second and third rows of Fig. 5 show example images for DB 1 and DB 2, respectively, taken from the monocular front-view camera. It can be seen that the test dataset includes various real driving situations such as tunnels, ramps, curves, and traffic congestions. Labels shown at the top of the images correspond to those shown on the map above the images. As shown in Table 1 and the images of Fig. 5, DB 2 is more complicated than DB 1, as there are more lane changes, longer tunnels, and traffic congestion. The digital map was built by a mobile mapping system (MMS). 3D points were automatically acquired by the MMS and landmark locations were manually designated using the 3D points. The detailed

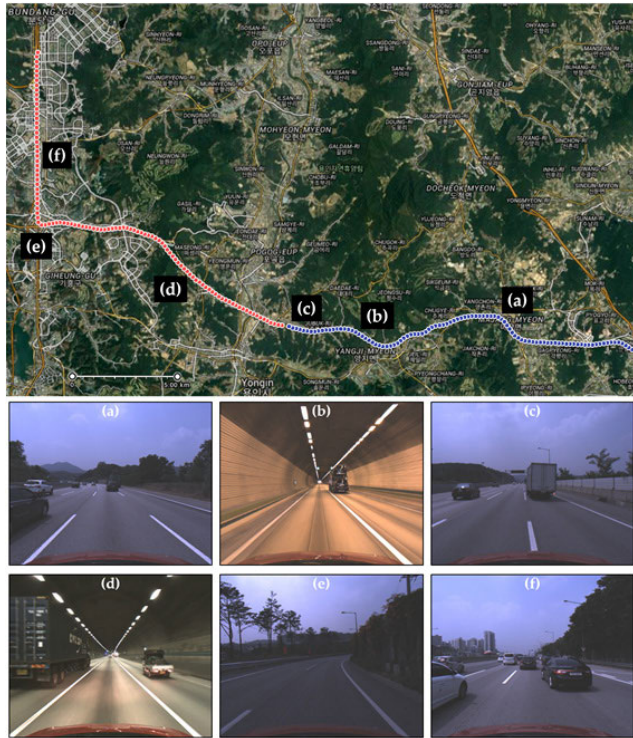


FIGURE 5. Test route and driving situations included in the test dataset. Blue and red points indicate the routes for DB 1 ((a), (b), and (c)) and DB 2 ((d), (e), and (f)), respectively. Labels shown at the top of the images correspond to those shown on the map above the images.

TABLE 1. Detailed explanations on the test dataset.

	DB 1	DB 2
Driving distance [km]	16.32	20.82
Average velocity [km/h]	71.11	65.98
Maximum velocity [km/h]	83.37	81.33
Tunnel distance [km]	0.73	1.50
Number of lane changes	1	7

explanations on the MMS and designation procedure are presented in [12].

The proposed system was quantitatively evaluated by comparing its localization results with outputs of a high-end positioning sensor (Applanix POS LV210 [39]). This positioning sensor consists of a real-time kinematic (RTK) GPS, high precision inertial measurement unit (IMU), and distance measurement indicator (DMI). This high-end positioning sensor was also used for the emulating GPS, wheel speed sensor, and yaw rate sensor. To this end, specifications of low-cost sensors presented in [6] were used. Frequency and horizontal position accuracy of the GPS were set to 1 Hz and 2.0 m, respectively. Sensor Fusion and Tracking Toolbox in MATLAB was used for GPS emulation. Noise (RMS) of the wheel speed and yaw rate sensors were set to 0.3 m/s and 0.5°/s, respectively, and their frequencies were set to 15 Hz. A monocular front-view camera located behind the windshield was used as a perception sensor. Its resolution,

horizontal field of view, and acquisition frequency are 1280 × 1024 pixels, 60°, and 15 Hz, respectively. The digital map was constructed by using a mobile mapping system (MMS) introduced in [12]. This digital map contains locations of lane markings, lane endpoints, and road sign centers and the types for each landmark.

B. PERFORMANCE EVALUATION AND COMPARISON

The proposed system was quantitatively evaluated and compared with previous approaches based on three positioning error criteria (lateral, longitudinal, Euclidean errors in terms of RMSE) and ego-lane identification accuracy. The lateral error indicates the position error in the direction perpendicular to the vehicle traveling direction, the longitudinal error indicates the position error in the vehicle traveling direction, and the Euclidean error indicates the Euclidean distance between the estimated and ground truth positions. In order to calculate the ego-lane identification accuracy, ego-lanes are assumed to be correctly identified when the lateral error is less than 1.75 m, which is half the minimum road width of a Korean highway (3.5 m). This is reasonable because the ego-vehicle mostly moves along the centerline of the lane. Since the particle filter involves randomness, the proposed system was applied to the test dataset 50 times and all evaluation results presented in this section were obtained from all 50 trials. As aforementioned, the proposed system identifies the ego-lane with the help of road signs. Thus, this system started at the location where road signs can be observed by the camera. Initial positions of the ego-vehicle were set by using a low-cost GPS, and initial particles were uniformly distributed with a width and height of 10 m centered around the ego-vehicle. The number of particles used for the particle filter was set to 1000.

Table 2 shows the performance evaluation result of the proposed system in both DB 1 and DB 2. This system gives less than 0.12 m for the lateral error, less than 0.25 m for the longitudinal error, less than 0.27 m for the Euclidean error in both DB 1 and DB 2. This accuracy can be considered sufficient for highway autonomous driving because the autonomous driving was successfully carried out with a Euclidean error of 0.54 m in [6]. The Euclidean error of DB 2 is slightly larger than that of DB 1. Compared with DB 1, DB 2 includes more roads (such as tunnels) with solid line lane markings where no lane endpoints are provided. Since the longitudinal positioning accuracy depends on the lane endpoints, their absence increases the longitudinal error of DB 2 and consequently increases its Euclidean error. In terms of the ego-lane identification rate, the proposed system achieves nearly 100%, which means it almost always provides a lateral error of less than 1.75 m in both DB 1 and DB 2.

Fig. 6 shows example localization results of the proposed system in DB 1 and DB 2. In this figure, (a) and (b) are from DB 1, and (c) and (d) are from DB 2. Upper and lower images in each figure show a driving situation and corresponding localization result, respectively. In the lower images, red points, blue crosses, and magenta triangles are localization

TABLE 2. Performance evaluation results of the proposed system.

DB	Lateral error (RMSE)	Longitudinal error (RMSE)	Euclidean error (RMSE)	Ego-lane identification rate
DB 1	0.12 m	0.18 m	0.21 m	100 %
DB 2	0.10 m	0.25 m	0.27 m	99.997 %

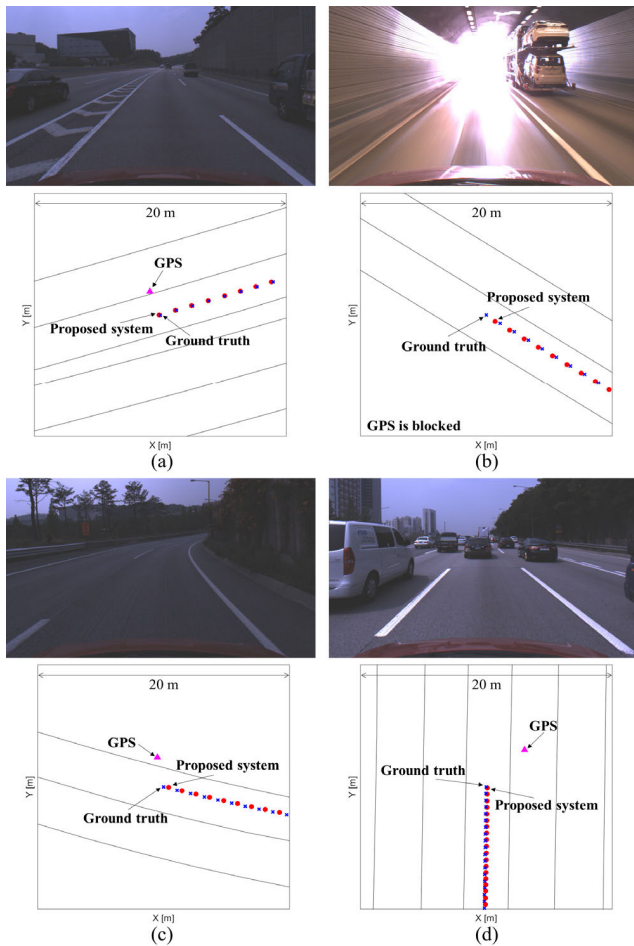


FIGURE 6. Example localization results of the proposed system. (a) and (b) are example results in DB 1, and (c) and (d) are example results in DB 2. Upper and lower images in each figure show a driving situation and corresponding localization result, respectively. In the lower images, red points, blue crosses, and magenta triangles are localization results of the proposed system, high precision positioning sensor, and low-cost GPS, respectively.

results of the proposed system, high precision positioning sensor, and low-cost GPS, respectively. Figures 6(a) to (d) shows a sloping road, tunnel, curved road, and congested road, respectively. The results in Table 2 and Fig. 6 reveal that precise lateral and longitudinal positions of the ego-vehicle can be obtained by the proposed system in various highway situations.

Fig. 7 shows detailed localization result of the proposed system in DB 1. In this figure, red and blue lines indicate the lateral and longitudinal errors, respectively. This system always achieves a lateral error less than 0.28 m thanks to road signs and lane markings. The road signs help ego-lane

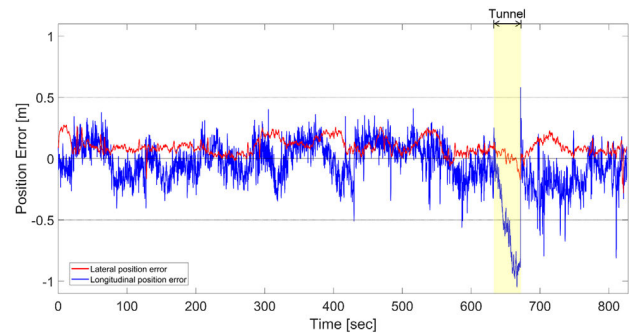


FIGURE 7. Detailed localization result of the proposed system in DB 1. Red and blue lines indicate the lateral and longitudinal errors, respectively.

identification and lane markings help in-lane lateral localization. Except for a yellow region between 630 and 670 seconds, this system mostly achieves a longitudinal error of less than 0.50 m thanks to the lane endpoints that help in-lane longitudinal localization. The yellow region between 630 and 670 seconds indicates the tunnel shown in Fig. 5(b), where only solid line lane markings exist. It can be noticed that the longitudinal error increases due to the absence of the lane endpoints. However, the longitudinal error decreases after the ego-vehicle exits the tunnel and observes the lane endpoints again. The longitudinal error can also increase when the lane endpoints are falsely detected. At 810 seconds in Fig. 7, some lane endpoints were false detected because of repainted lane markings and this increased the longitudinal error up to 0.81 m.

In general highway driving situations, the most frequent landmark is lane markings. Thus, the ego-vehicle can easily estimate its in-lane lateral position based on lane markings. The second most frequent landmark is lane endpoints. The ego-vehicle can estimate its in-lane longitudinal position based on lane endpoints. Road signs are less common than the other landmarks. However, road signs almost always appear at highway entrances. Thus, the ego-lane can be identified based on road signs soon after the ego-vehicle enters the highway. Once the ego-lane is identified, the ego-vehicle can keep its positioning accuracy by updating the particles based on lane markings, lane endpoints, GPS, and in-vehicle motion sensors, even though road signs are unobservable for a while.

The proposed system was compared with two representative vehicle localization approaches. One approach uses GPS with DR, and the other approach utilizes GPS, DR, lane markings, and a digital map. These approaches are abbreviated as GPS-DR and GPS-DR-LANE in this section, respectively. For fair comparison, the proposed system,

TABLE 3. Performance evaluation results of the three approaches.

DB	Approach	Lateral error (RMSE)	Longitudinal error (RMSE)	Euclidean error (RMSE)	Ego-lane identification rate
DB 1	GPS-DR	2.45 m	1.41 m	2.84 m	58.22 %
	GPS-DR-LANE	1.64 m	1.44 m	2.70 m	81.92 %
	Proposed system	0.12 m	0.18 m	0.21 m	100 %
DB 2	GPS-DR	4.12 m	1.47 m	4.42 m	54.18 %
	GPS-DR-LANE	0.96 m	1.44 m	1.96 m	78.49 %
	Proposed system	0.10 m	0.25 m	0.27 m	99.997 %

GPS-DR, and GPS-DR-LANE were performed under the same conditions using the particle filter. Table 3 shows performance comparison results of three approaches. In both DB 1 and DB 2, GPS-DR shows the worst performance, GPS-DR-LANE shows the next worst performance, and the proposed system shows the best performance in terms of Euclidean error. Performance difference between GPS-DR and GPS-DR-LANE is caused by the decrease of the lateral error when using lane markings. In DB 1, the use of lane markings decreases the lateral error from 2.45 m to 1.64 m while the longitudinal error remains almost the same (1.41 m and 1.44 m). Although lane markings are utilized, GPS-DR-LANE gives large lateral and longitudinal errors. This is because lane markings have a drawback of lacking information on ego-lane identification and longitudinal position estimation. This is the reason why the proposed system tries to utilize the lane endpoints and road signs. As shown in Table 3, the proposed system dramatically increases the localization performance compared with GPS-DR-LANE. This performance difference is caused by the decrease of the lateral error with the help of the road signs and the decrease of the longitudinal error with the help of the lane endpoints. In DB 1, the use of the road signs decreases the lateral error from 1.64 m to 0.12 m and the use of the lane endpoints decreases the longitudinal error from 1.44 m to 0.18 m. In terms of the ego-lane identification rate, the proposed system outperforms the other two approaches by showing 100 % while GPS-DR and GPS-DR-LANE show 58.22 % and 81.92 % in DB 1, respectively. Since the ego-lane identification rate highly depends on the lateral error, this result shows that road signs and lane markings can increase lateral positioning performance and consequently help ego-lane identification. As shown in Table 3, the performance differences between the three approaches in DB 2 are almost the same as those in DB 1.

Recently, Kim *et al.* [26] performed vehicle localization in Korean motorway roads, which are similar to our test environment. Their system utilizes lane markings detected by the monocular front-view camera and streetlights detected by a high-end Lidar with 16 layers, which has never been mass-produced by attaching them to off-the-shelf vehicles. It achieves a lateral error of 0.21 m and longitudinal error of 0.63 m. Compared with this system, the proposed system achieves more accurate results despite using only a

TABLE 4. Execution time of the proposed system.

	DB 1	DB 2	Average
Execution time	4.45 ms	4.24 ms	4.34 ms
Frame rate	225 fps	236 fps	230 fps

monocular front-view camera, which is a low-end perception sensor that has been widely attached to various off-the-shelf vehicles.

C. EXECUTION TIME

Execution times of the proposed system are presented in Table 4. These times were measured on an Intel Core i7-7700 CPU with 16 GB RAM using only a single core. An average execution time of 4.34 ms was required for the proposed system, which means that 230 frames can be processed per second in real time. Processing times for detecting lane markings, lane endpoints, and road signs are excluded in Table 4 because these tasks are conducted not by a vehicle localization module but by a multi-functional front-view camera module. Since only a small amount of computation cost is required for the proposed system, this system can readily be applied to off-the-shelf vehicles.

VII. CONCLUSIONS

This paper proposes a practical and low-cost vehicle localization system targeted to highway situations. The proposed system effectively fuses various low-cost sensors such as a monocular front-view camera, low-end GPS, and in-vehicle motion sensors along with a digital map in the particle filter framework. Compared with previous approaches, this system utilizes two additional landmarks (lane endpoints and road signs) to improve both longitudinal positioning and ego-lane identification accuracies. Experimental results show that the proposed system achieves vehicle localization results sufficient for highway autonomous driving and outperforms previous approaches while requiring only a tiny amount of computational cost. Furthermore, this system uses only low-cost sensors that have been widely mounted on off-the-shelf vehicles. Because it has obvious advantages from a practical viewpoint, we are currently modifying and optimizing the whole system including landmark detection and vehicle

localization and will implement it using a low-cost embedded board such as NXP330Q processor, an automotive multimedia application processor.

ACKNOWLEDGMENT

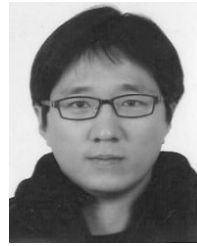
(Mi Jin Choi and Jae Kyu Suhr contributed equally to this work.)

REFERENCES

- [1] H. Cai, Z. Hu, G. Huang, D. Zhu, and X. Su, "Integration of GPS, monocular vision, and high definition (HD) map for accurate vehicle localization," *Sensors*, vol. 18, no. 10, p. 3270, Sep. 2018.
- [2] S. H. Lee and C. C. Chung, "Robust multirate on-road vehicle localization for autonomous highway driving vehicles," *IEEE Trans. Control Syst. Technol.*, vol. 25, no. 2, pp. 577–589, Mar. 2017.
- [3] R. P. D. Vivacqua, M. Bertozzi, P. Cerri, F. N. Martins, and R. F. Vassallo, "Self-localization based on visual lane marking maps: An accurate low-cost approach for autonomous driving," *IEEE Trans. Intell. Transp. Syst.*, vol. 19, no. 2, pp. 582–597, Feb. 2018.
- [4] J. K. Suhr, J. Jang, D. Min, and H. G. Jung, "Sensor fusion-based low-cost vehicle localization system for complex urban environments," *IEEE Trans. Intell. Transp. Syst.*, vol. 18, no. 5, pp. 1078–1086, May 2017.
- [5] C. Li, Z. Hu, Z. Li, Y. Ma, and M. A. Sotelo, "Multiscale site matching for vision-only self-localization of intelligent vehicles," *IEEE Intell. Transp. Syst. Mag.*, vol. 10, no. 3, pp. 170–183, Jun. 2018.
- [6] K. Jo, Y. Jo, J. K. Suhr, H. G. Jung, and M. Sunwoo, "Precise localization of an autonomous car based on probabilistic noise models of road surface marker features using multiple cameras," *IEEE Trans. Intell. Transp. Syst.*, vol. 16, no. 6, pp. 3377–3392, Dec. 2015.
- [7] A. Hata and D. Wolf, "Feature detection for vehicle localization in urban environments using a multilayer LIDAR," *IEEE Trans. Intell. Transp. Syst.*, vol. 17, no. 2, pp. 420–429, Feb. 2016.
- [8] K. Yoneda, H. Tehrani, T. Ogawa, N. Hukuyama, and S. Mita, "Lidar scan feature for localization with highly precise 3-D map," in *Proc. IEEE Intell. Vehicles Symp.*, Jun. 2014, pp. 1345–1350.
- [9] M. Stübler, J. Wiest, and K. Dietmayer, "Feature-based mapping and self-localization for road vehicles using a single grayscale camera," in *Proc. IEEE Intell. Vehicles Symp. (IV)*, Jun. 2015, pp. 267–272.
- [10] S. Nedeveschi, V. Popescu, R. Danescu, T. Marita, and F. Oniga, "Accurate ego-vehicle global localization at intersections through alignment of visual data with digital map," *IEEE Trans. Intell. Transp. Syst.*, vol. 14, no. 2, pp. 673–687, Jun. 2013.
- [11] D. Gruyer, R. Belaroussi, and M. Revilloud, "Accurate lateral positioning from map data and road marking detection," *Expert Syst. Appl.*, vol. 43, pp. 1–8, Jan. 2016.
- [12] E. S. Jang, J. K. Suhr, and H. G. Jung, "Lane endpoint detection and position accuracy evaluation for sensor fusion-based vehicle localization on highways," *Sensors*, vol. 18, no. 12, p. 4389, Dec. 2018.
- [13] H.-Y. Cheng, C.-C. Yu, C.-L. Lin, H.-C. Shih, and C.-W. Kuo, "Ego-lane position identification with event warning applications," *IEEE Access*, vol. 7, pp. 14378–14386, 2019.
- [14] S. Lee, S.-W. Kim, and S.-W. Seo, "Accurate ego-lane recognition utilizing multiple road characteristics in a Bayesian network framework," in *Proc. IEEE Intell. Vehicles Symp. (IV)*, Jun. 2015, pp. 543–548.
- [15] Y.-W. Seo and R. Rajkumar, "Tracking and estimation of ego-vehicle's state for lateral localization," in *Proc. 17th Int. IEEE Conf. Intell. Transp. Syst. (ITSC)*, Oct. 2014, pp. 1251–1257.
- [16] S. Kim and S. Y. Park, "Lane-level positioning based on 3D tracking path of traffic signs," in *Proc. 11th Joint Conf. Comput. Vis., Imag. Comput. Graph. Theory Appl.*, 2016, pp. 642–648.
- [17] K. Choi, J. K. Suhr, and H. G. Jung, "FAST pre-filtering-based real time road sign detection for low-cost vehicle localization," *Sensors*, vol. 18, p. 3590, Oct. 2018.
- [18] C. Jang, S. Cho, S. Jeong, J. K. Suhr, H. G. Jung, and M. Sunwoo, "Traffic light recognition exploiting map and localization at every stage," *Expert Syst. Appl.*, vol. 88, pp. 290–304, Dec. 2017.
- [19] N. Mattern, R. Schubert, and G. Wanielik, "High-accurate vehicle localization using digital maps and coherency images," in *Proc. IEEE Intell. Vehicles Symp.*, Jun. 2010, pp. 462–469.
- [20] J. Levinson and S. Thrun, "Robust vehicle localization in urban environments using probabilistic maps," in *Proc. IEEE Int. Conf. Robot. Automat.*, May 2010, pp. 4372–4378.
- [21] M. Schreiber, C. Knöppel, and U. Franke, "LaneLoc: Lane marking based localization using highly accurate maps," in *Proc. IEEE Intell. Vehicles Symp.*, Jun. 2013, pp. 449–454.
- [22] H. Deusch, J. Wiest, S. Reuter, D. Nuss, M. Fritzsche, and K. Dietmayer, "Multi-sensor self-localization based on maximally stable extremal regions," in *Proc. IEEE Intell. Vehicles Symp.*, Jun. 2014, pp. 555–560.
- [23] D. Kim, T. Chung, and K. Yi, "Lane map building and localization for automated driving using 2D laser rangefinder," in *Proc. IEEE Intell. Vehicles Symp. (IV)*, Jun. 2015, pp. 680–685.
- [24] W. Lu, E. Seigne, F. S. A. Rodriguez, and R. Reynaud, "Lane marking based vehicle localization using particle filter and multi-kernel estimation," in *Proc. 3th Int. Conf. Control Automat. Robot. Vis. (ICARCV)*, Dec. 2014, pp. 601–606.
- [25] H. Li, F. Nashashibi, and G. Toulminet, "Localization for intelligent vehicle by fusing mono-camera, low-cost GPS and map data," in *Proc. 13th Int. IEEE Conf. Intell. Transp. Syst.*, Sep. 2010, pp. 1657–1662.
- [26] C. Kim, S. Cho, M. Sunwoo, and K. Jo, "Crowd-sourced mapping of new feature layer for high-definition map," *Sensors*, vol. 18, no. 12, p. 4172, Dec. 2018.
- [27] A. Y. Hata, F. S. Osorio, and D. F. Wolf, "Robust curb detection and vehicle localization in urban environments," in *Proc. IEEE Intell. Vehicles Symp.*, Jun. 2014, pp. 1257–1262.
- [28] M. Lundgren, E. Stenborg, L. Svensson, and L. Hammarstrand, "Vehicle self-localization using off-the-shelf sensors and a detailed map," in *Proc. IEEE Intell. Vehicles Symp.*, Jun. 2014, pp. 522–528.
- [29] K. Jo, K. Chu, and K. Sunwoo, "GPS-bias correction for precise localization of autonomous vehicles," in *Proc. IEEE Intell. Vehicles Symp.*, Jun. 2013, pp. 636–641.
- [30] T. Wu and A. Ranganathan, "Vehicle localization using road markings," in *Proc. IEEE Intell. Vehicles Symp.*, Jun. 2013, pp. 1185–1190.
- [31] V. Balali, A. A. Rad, and M. Golparvar-Fard, "Detection, classification, and mapping of U.S. traffic signs using Google street view images for roadway inventory management," *Vis. Eng.*, vol. 3, p. 15, Dec. 2015.
- [32] Y. Yang, H. Luo, H. Xu, and F. Wu, "Towards real-time traffic sign detection and classification," *IEEE Trans. Intell. Transp. Syst.*, vol. 17, no. 7, pp. 2022–2031, Jul. 2016.
- [33] H. Luo, Y. Yang, B. Tong, F. Wu, and B. Fan, "Traffic sign recognition using a multi-task convolutional neural network," *IEEE Trans. Intell. Transp. Syst.*, vol. 19, no. 4, pp. 1100–1111, Apr. 2018.
- [34] H. S. Lee and K. Kim, "Simultaneous traffic sign detection and boundary estimation using convolutional neural network," *IEEE Trans. Intell. Transp. Syst.*, vol. 19, no. 5, pp. 1652–1663, May 2018.
- [35] S. Thrun, W. Burgard, and D. Fox, *Probabilistic Robotics*. Cambridge, MA, USA: MIT Press, 2005.
- [36] F. Gustafsson, "Particle filter theory and practice with positioning applications," *IEEE Aerosp. Electron. Syst. Mag.*, vol. 25, no. 7, pp. 53–82, Jul. 2010.
- [37] L. Tiancheng, B. Miodrag, and D. M. Petar, "Resampling methods for particle filtering: Classification, implementation, and strategies," *Signal Process. Mag.*, vol. 32, no. 3, pp. 70–86, May 2015.
- [38] H. W. Kuhn, "The Hungarian method for the assignment problem," *Naval Res. Logistics Quart.*, vol. 2, nos. 1–2, pp. 83–97, Mar. 1955.
- [39] *Applanix POS LV 210*. Accessed: Nov. 8, 2018. [Online]. Available: <https://www.applanix.com/products/poslv.htm>
- [40] J.-Z. Yuan, H. Chen, B. Zhao, and Y. Xu, "Estimation of vehicle pose and position with monocular camera at urban road intersections," *J. Comput. Sci. Technol.*, vol. 32, no. 6, pp. 1150–1161, Nov. 2017.
- [41] Y. Gu, L.-T. Hsu, and S. Kamijo, "Passive sensor integration for vehicle self-localization in urban traffic environment," *Sensors*, vol. 15, no. 12, pp. 30199–30220, Dec. 2015.
- [42] C. Yuan, H. Chen, J. Liu, D. Zhu, and Y. Xu, "Robust lane detection for complicated road environment based on normal map," *IEEE Access*, vol. 6, pp. 49679–49689, 2018.



MI JIN CHOI received the B.Sc. and M.Sc. degrees in mechanical engineering from Hankyong National University, Anseong, South Korea, in 2015 and 2018, respectively. She is currently a full-time Researcher with Sejong University, Seoul, South Korea. Her research interests include localization, inertial-sensing-based tracking, and sensor fusion for intelligent vehicles.



KYOUNGTAEK CHOI received the B.S. degree in electronic engineering from Chungang University, Seoul, South Korea, in 2001, and the M.S. and Ph.D. degrees in electrical and electronic engineering from Yonsei University, Seoul, South Korea, in 2003 and 2008, respectively. From March 2008 to June 2009, he was a full-time Researcher and a Research Professor with Yonsei University. From August 2009 to November 2013, he was with Lignex1 Corporation Research and Development Center, where he developed un-manned vehicle systems and detection/tracking algorithms applied to ship-to-ship missiles. From December 2013 to April 2016, he was with the Samsung S1 Research and Development Center, where he developed a surveillance system. And he developed a safety environment monitoring system for a factory and a traffic accident monitoring system. From May 2016 to February 2019, he was a Research Professor with the Korea National Korea National University of Transportation. He is currently an Assistant Professor with the School of Intelligent Mechatronics Engineering, Sejong University, Seoul. His research interests include computer vision, pattern recognition, object tracking, vehicle localization, and embedded system implementation for intelligent vehicles.



JAE KYU SUHR (M'12) received the B.S. degree in electronic engineering from Inha University, Incheon, South Korea, in 2005, and the M.S. and Ph.D. degrees in electrical and electronic engineering from Yonsei University, Seoul, South Korea, in 2007 and 2011, respectively. From 2011 to 2016, he was with the Automotive Research Center, Hanyang University, Seoul. From 2016 to 2017, he was with the Korea National University of Transportation, Chungju, South Korea. He is currently an Assistant Professor with the School of Intelligent Mechatronics Engineering, Sejong University, Seoul. His research interests include computer vision, image analysis, pattern recognition, and sensor fusion for intelligent vehicles.



HO GI JUNG (M'05–SM'10) received the B.E., M.E., and Ph.D. degrees in electronic engineering from Yonsei University, Seoul, South Korea, in 1995, 1997, and 2008, respectively. From 1997 to April 2009, he was with MANDO Corporation Global Research and Development Headquarters, where he developed environmental recognition systems for various driver assistant systems. From May 2009 to February 2011, he was a full-time Researcher and a Research Professor with Yonsei University. From March 2011 to July 2016, he was an Assistant Professor with Hanyang University, Seoul, South Korea. Since August 2016, he has been an Associate Professor with the Korea National University of Transportation, Chungju, South Korea. He is working on recognition systems for intelligent vehicles. His research interests include recognition systems for intelligent vehicles, next-generation vehicles, computer vision applications, and pattern recognition applications. Dr. Jung is an Associate Editor of the IEEE TRANSACTIONS ON INTELLIGENT TRANSPORTATION SYSTEMS and the IEEE TRANSACTIONS ON INTELLIGENT VEHICLES.

...